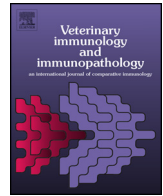




Since January 2020 Elsevier has created a COVID-19 resource centre with free information in English and Mandarin on the novel coronavirus COVID-19. The COVID-19 resource centre is hosted on Elsevier Connect, the company's public news and information website.

Elsevier hereby grants permission to make all its COVID-19-related research that is available on the COVID-19 resource centre - including this research content - immediately available in PubMed Central and other publicly funded repositories, such as the WHO COVID database with rights for unrestricted research re-use and analyses in any form or by any means with acknowledgement of the original source. These permissions are granted for free by Elsevier for as long as the COVID-19 resource centre remains active.



Technical Report

Evaluation of a panel of antibodies for the immunohistochemical identification of immune cells in paraffin-embedded lymphoid tissues of new- and old-world camelids



Ann-Kathrin Uhde^a, Annika Lehmbecker^{a,b}, Wolfgang Baumgärtner^{a,b,*}, Ingo Spitzbarth^{a,b}

^a Department of Pathology, University of Veterinary Medicine Hannover Foundation, Bünteweg 17, 30559, Hannover, Germany

^b Center for Systems Neuroscience, Bünteweg 2, 30559, Hannover, Germany

ARTICLE INFO

Article history:

Received 17 October 2016

Received in revised form

28 December 2016

Accepted 12 January 2017

Keywords:

Immunohistochemistry

T cells

B cells

Macrophages

Camelids

Llama

Alpaca

Bactrian

Dromedary

ABSTRACT

Different species of camelids play an important role in the epidemiology of various emerging infectious diseases such as Middle East respiratory syndrome. For precise investigations of the immunopathogenesis in these host species, appropriate immunohistochemical markers are highly needed in order to phenotype distinct immune cells populations in camelids. So far, specific immunohistochemical markers for camelid immune cells are rarely commercially available, and cross-reactivity studies are restricted to the use of frozen dromedary tissues. To bridge this gap, 14 commercially available primary antibodies were tested for their suitability to demonstrate immune cell populations on formalin fixed paraffin-embedded (FFPE) tissue sections of dromedaries, Bactrian camels, llamas, and alpacas in the present study. Out of these, 9 antibodies directed against CD3, CD20, CD79 α , HLA-DR, Iba-1, myeloid/histiocyte antigen, CD204, CD208, and CD68 antigen exhibited distinct immunoreaction patterns to certain camelid immune cell subsets. The distribution of these antigens was comparatively evaluated in different anatomical compartments of thymus, spleen, mesenteric, and tracheobronchial lymph nodes. The presented results will provide a basis for further investigations in camelids, especially with respect to the role of the immune response in certain infectious diseases, which harbor a considerable risk to spill over to other species.

© 2017 Elsevier B.V. All rights reserved.

1. Introduction

The numbers of alpacas (*Vicugna pacos*) and llamas (*Lama glama*) housed as companion animals is substantially increasing (Riek et al., 2013). Similarly, dromedaries (*Camelus dromedarius*) represent an important livestock species in both Africa and Asia and especially

on the Arabian Peninsula, where they serve as a major source of milk and meat (Burger, 2016).

In 2012 a single-stranded, positive-sensed beta-coronavirus was isolated in the Kingdom of Saudi Arabia (Chan et al., 2015; van Boheemen et al., 2012; Zaki et al., 2012). Until today Middle East respiratory syndrome coronavirus (MERS-CoV) spread to 27 countries and caused more than 1,800 laboratory-confirmed cases of pneumonia including 643 fatal progressions in man (World Health Organization (2016) Middle East respiratory syndrome coronavirus. Available at www.who.int/emergencies/mers-cov/en/. Accessed October 06, 2016). Recent studies indicate that dromedaries appear to play a pivotal epidemiological role in transmitting the virus to humans, and experimental studies with dromedaries illustrate shedding of MERS-CoV after intranasal inoculation (Adney et al., 2014; Haagmans et al., 2015; Reusken et al., 2013). However, there is a high demand for additional animal models, including the use of llamas and alpacas, which allow sophisticated pathological investigations in order to determine details of pathogenesis, cell tropism, and viral transmission of MERS-CoV. Besides MERS-CoV infections, dromedaries and Bactrian camels (*Camelus ferus*) also play a sig-

Abbreviations: CD, cluster of differentiation; DALT, dense nodular lymphoid tissue; DC(s), Dendritic cell(s); DLT, diffuse lymphoid tissue; FFPE, formalin-fixed paraffin-embedded; Foxp3, forkhead box P3; GAM, goat anti-mouse Immunoglobulin G; GAR, goat anti-rabbit Immunoglobulin G; H&E, hematoxylin and eosin; HLA, human leucocyte antigen; Iba-1, ionized calcium-binding adapter molecule 1; IgG, Immunoglobulin G; IHC, immunohistochemistry; LN, lymphoid nodules; mc, monoclonal; MERS-CoV, Middle East respiratory syndrome coronavirus; MUM1, multiple myeloma oncogene 1; PALS, periarteriolar lymphoid sheath; Pax-5, paired box protein 5; PBS, phosphate buffered saline; pc, polyclonal; RAR, rabbit anti-rat Immunoglobulin G; RT, room temperature.

* Corresponding author at: Department of Pathology, University of Veterinary Medicine Hannover Foundation, Bünteweg 17, 30559, Hannover, Germany.

E-mail address: Wolfgang.Baumgaertner@tiho-hannover.de (W. Baumgärtner).

nificant epidemiological role in other emerging infectious diseases such as West Nile Virus encephalitis (Joseph et al., 2016), Hepatitis E Virus infections (Rasche et al., 2016), and rabies (Feng et al., 2014; Liu et al., 2016), demonstrating that naturally occurring and experimentally induced diseases in old and new world camelids might emerge as important animal models for studies upon the pathogenesis of such zoonotic infections.

The use of commercially available mono (mc)- and polyclonal (pc) antibodies in immunohistochemistry (IHC) has substantially improved our knowledge about the immunopathogenesis of pathological processes in a broad range of species and diseases (Duraiyan et al., 2012). Primary antibodies detecting specific human and murine antigens can often be used successfully for the detection of conserved epitopes on tissues of various animals, including both domestic and exotic wild life species (Faldyna et al., 2007; Heinrich et al., 2015; Salvadori et al., 2016; Seibel et al., 2010).

Earlier studies have tested a limited panel of antibodies, mainly for the detection of lymphocytes, and were carried out on frozen tissue in only one camelid species (dromedary; Zidan and Pabst, 2004, 2012; Zidan et al., 2000b). In another study, one B cell marker (Pax-5) and one T cell marker (CD3) were used on paraffin embedded gut associated lymphoid tissue (GALT) of alpacas, experimentally infected with bovine viral diarrhoea virus (Steffen et al., 2014). However, the establishment of a broader panel of immunohistochemical markers on formalin fixed paraffin embedded (FFPE) tissue represents a prerequisite to elucidate the role of the immune response in diseases of camelids. Therefore, it was the aim of the present study to test the applicability of commercially available immunohistochemical markers for the detection of immune cells in new- and old-world camelids in FFPE tissue of different lymphoid organs to provide a solid fundament for further research on healthy and diseased camelids with special respect to prospective spill-over infections.

2. Materials and methods

2.1. Animals and tissue samples

Tissues used in the present study were taken from the archive of the Department of Pathology, University of Veterinary Medicine Hannover. A complete necropsy was performed and sampled organs were fixed in 10% non-neutral buffered formalin for 24 h and routinely embedded for histology. The archive was screened for cases of new- and old world camelids, in which lymphoid organs were available. Briefly, formalin fixed tissues were automatically dehydrated by an ascending alcohol series using the embedding machine Thermo Scientific™ Shandon™ Pathcentre™ (Thermo Fisher Scientific, Langenselbold, Germany) and subsequently embedded in paraffin. 4 µm thick paraffin sections of lymphoid organs were stained with H&E and examined by routine light microscopy. Lymphoid tissues affected by destruction of organotypic architecture and/or major lesions such as severe suppurative inflammation, abscess or granuloma formation, and neoplastic processes were excluded from the present study. Moreover, lymphoid organs with severe lymphoid depletion and marked auto- and heterolytic changes were omitted from further processing. Overall, the lowest number of lymphoid organs fulfilling the inclusion criteria was available from dromedaries. In particular, 5 spleens, 5 mesenteric lymph nodes, and 5 tracheobronchial lymph nodes of dromedary origin were obtainable. The number of lymphoid tissues from the remaining species (Bactrian camels, llamas, and alpacas) was consequently adjusted to n=5 for each of the aforementioned organs. Accordingly, in total 20 spleens and 20 tracheobronchial and 20 mesenteric lymph nodes were investigated in the present study (5 per species for each organ). Additionally, thy-

mus tissue was available from two young animals of each species (8 animals with a median age of 3 days).

2.2. Immunohistochemistry

For IHC a panel of different antibodies (n = 14) was applied on lymph nodes of each species to screen for their general suitability for camelid lymphoid tissue (Table 1). The tested antibodies have previously been reported to cross-react with canine and bovine immune cells, respectively (Ackermann et al., 1994; Alldinger et al., 1996; Fernandez et al., 2017; Kato et al., 2013; Pierezan et al., 2014; Ramos-Vara et al., 2007; Romero-Palomo et al., 2013; Spitzbarth et al., 2011; Wünschmann et al., 2000). Consequently, archived FFPE sections from mesenteric lymph nodes of a dog or an ox were used as positive controls. IHC was performed by use of the avidin-biotin-peroxidase complex method as described previously (Alldinger et al., 1996). Briefly, after dewaxing by incubating the sections for 5 min twice in Rotoclear® (Roth C. GmbH & Co. KG, Karlsruhe, Germany) and rehydration in isopropanol and ethanol (96%; each for 5 min), endogenous peroxidase activity was blocked by incubation of sections in 85% ethanol with 0.5% H₂O₂ for 30 min at room temperature (RT). If necessary (Table 1), pretreatment was either done by incubating the sections in citrate buffer (2.1 g citric acid monohydrate in 1 l distilled water, adjusted with NaOH to pH = 6.0) for 20 min in a microwave (800 W) or with 20 min pronase treatment at 37 °C (pronase E, 50 mg in 100 ml phosphate buffered saline [PBS] and 0.1 g CaCl₂ × 2H₂O with pH adjusted to 7.2). Subsequently, sections were transferred to Shandon Coverplates™ (Thermo Electron GmbH, Dreieich, Germany). To block unspecific binding, inactivated normal rabbit serum (for CD208 and Foxp3) or normal goat serum (all other antibodies) was applied for 30 min in a dilution of 1:5 with PBS (pH 7.2). For appropriate negative controls, primary antibodies (Table 1) were replaced by ascites fluid from Balb/c mice (1:1000; CD79α, Pax-5, MUM1 protein, HLA-DR antigen, CD68, myeloid/histiocyte antigen, CD204, CD205), rabbit (1:3000; CD3, CD20, Iba-1, lysozyme), and rat serum (1:1000; Foxp3, CD208), respectively. After 90 min of incubation at RT and subsequent washing with PBS, the appropriate secondary biotinylated antibody was added in a dilution of 1:200 with PBS. Incubation for 60 min at RT was followed by treatment with the avidin-biotin-peroxidase complex (Vectastain ABC Kit Standard, Vector Laboratories, Burlingame, California, USA) according to the manufacturer's protocol. Visualization of the reaction was achieved by the chromogen 3,3'-diaminobenzidine tetrahydrochloride (DAB, 0.05%, Sigma Aldrich Chemie GmbH, Taufkirchen, Germany) with addition of 0.03% H₂O₂. Slides were finally slightly counterstained with Mayer's hematoxylin (Roth C. GmbH & Co KG, Karlsruhe, Germany).

2.3. Evaluation and quantification

Sections were viewed under an Olympus BX-51 digital camera microscope (Olympus Optical Co., Hamburg, Germany). Positive immunoreactivity was appreciated if cellular staining pattern and cellular morphology fitted with the expected distribution pattern and immunoreactivity appearance of the positive control. All antibodies, which produced positive results on camelid lymph nodes, were applied to serial sections of lymph node, spleen, and thymus of all examined camelid species and comparatively assessed according to a semiquantitative scoring system (Heinrich et al., 2015). For all camelid species, scoring was adapted to the anatomical compartments of dromedary lymph nodes, which are known to differ from other mammals in some aspects (Abdel-Magied et al., 2001; Zidan et al., 2000a; Zidan and Pabst, 2004; Zidan and Pabst, 2012). Within sections of spleens, positive immunoreactivity was differentially evaluated for the periarteriolar lymphoid sheaths (PALS), follicles,

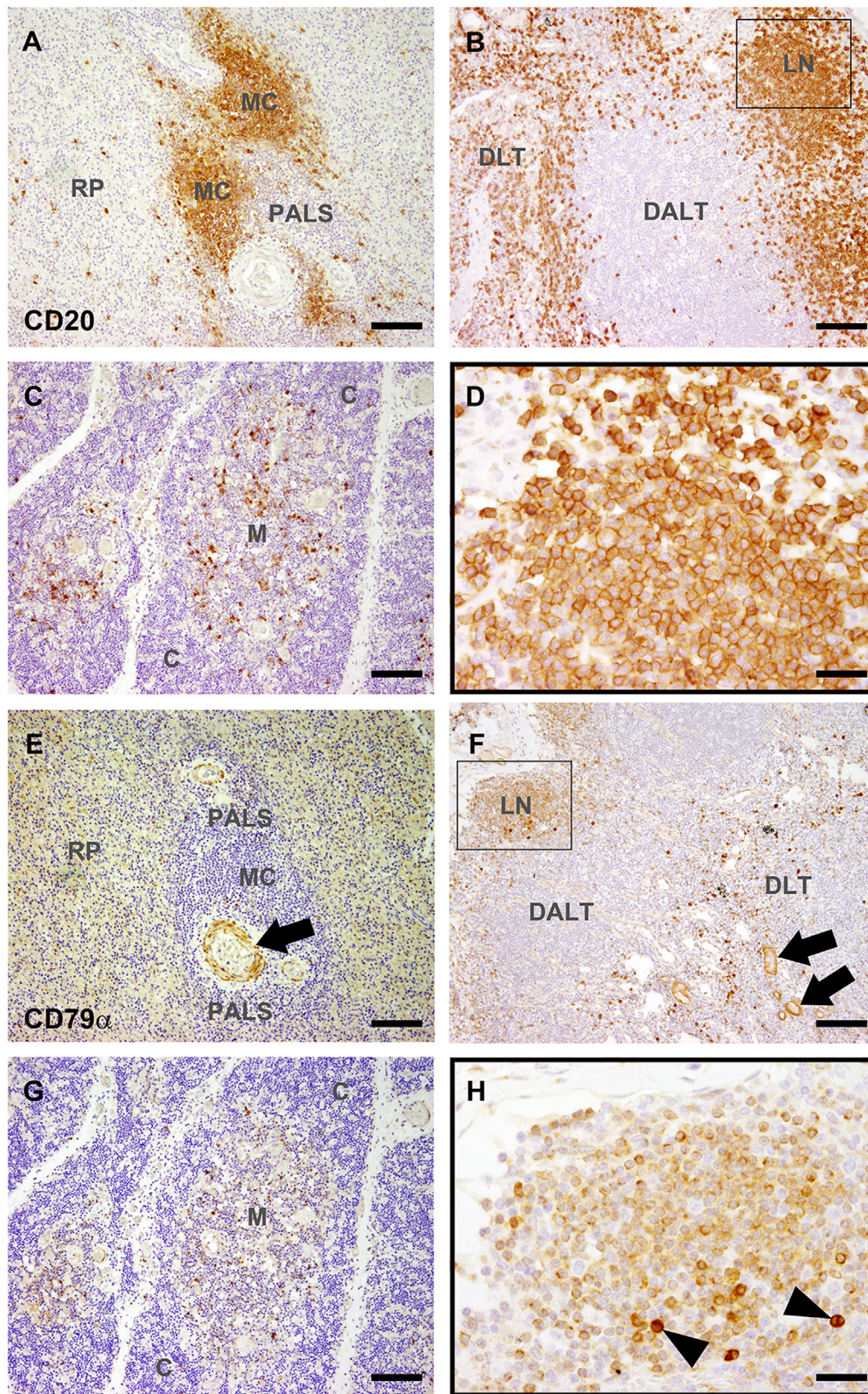


Fig. 1. Representative immunohistochemical reactions for detection of B cell populations in the spleen, lymph node, and thymus of a Bactrian camel (A–D: CD20; E–H: CD79 α). Avidin-biotin-peroxidase complex method with 3,3'-diaminobenzidine as chromogen. (A) CD20; spleen. CD20 positive cells with distinct membrane-bound signal and lymphoid morphology, suspicious of B cells, are mainly located in Malpighian corpuscles (MC) adjacent to the periarteriolar lymphoid sheath (PALS), while only scattered immunopositive cells are seen throughout the red pulp (RP). Scale bar = 100 μ m. (B) CD20; lymph node. CD20 positive cells are not only located in lymphoid nodules (LN), which resemble the B cell compartment, but there are also low numbers of cells with lymphoid morphology positioned within dense anodular lymphoid tissue (DALT; T cell compartment) and diffuse lymphoid tissue (DLT). Scale bar = 100 μ m. (C) CD20; thymus. Scattered CD20 immunopositive cells are noted within the thymic medulla (M), while there is no immunoreaction within the thymic cortex (C). Scale bar = 100 μ m. (D) CD20; lymph node. Higher magnification of the inset in (B). Morphologically, CD20

Table 1
Antigen, clonality, species, source, dilution, antigen retrieval and secondary antibodies used for IHC.

antigen	clonality, clone, species	source	dilution	antigen retrieval	secondary Ab	result
CD3	pc, rabbit	DakoCytomation	1:500	Citrat	GAR	+
CD79α	mc, HM57, mouse	Abcam	1:5000	Citrat	GAM	(+)
CD20	pc, rabbit	Thermo Fisher scientific	1:200	Citrat	GAR	+
Pax-5	mc, 24/Pax-5, mouse	BD Biosciences	1:10	#	GAM	–
Mum1	mc, MUM1p, mouse	DakoCytomation	1:10	#	GAM	–
Foxp3	mc, FJK-16s, rat	eBioscience	1:10	#	RAR	–
HLA-DR	mc, TAL.1B5, mouse	DakoCytomation	1:100	Citrat	GAM	+
Iba-1	pc, rabbit	Wako	1:500	Citrat	GAR	+
CD68	mc, KP1, mouse	DakoCytomation	1:100	Citrat	GAM	+
Myeloid/histiocyteantigen	mc, MAC387, mouse	DakoCytomation	1:500	Citrat	GAM	+
CD204	mc, SRA-E5, mouse	Transgenic Inc.	1:1000	Citrat	GAM	+
CD205	mc, CC98, mouse	AbD Serotec	1:10	#	GAM	–
CD208	mc, 1010E1.01, rat	Dendritics	1:200	Citrat	RAR	+
Lysozyme	pc, rabbit	Dako	1:10	#	GAR	–

CD, cluster of differentiation; Pax-5, paired box protein 5; MUM1, multiple myeloma oncogene 1; Foxp3, forkhead box P3, HLA, human leucocyte antigen; Iba-1, ionized calcium-binding adapter molecule 1; pc, polyclonal; mc, monoclonal; #, antigen retrieval was performed with boiling citrate buffer, pronase, and omission of pretreatment; GAR, goat anti-rabbit Immunoglobulin G (IgG); GAM, goat anti-mouse IgG; RAR, rabbit anti-rat IgG; +, positive; –, negative; (+) the antibody displayed a distinct immunoreaction on certain cells, but there was considerable background staining, false nuclear reactions, and the number of labeled cells was significantly lower than in the positive control of canine tissue.

Table 2
Distribution of antigens in different compartments of spleen.

Detected antigen	Follicles				PALS				Red Pulp Cords				Red pulp Sinuses			
	L	A	D	C	L	A	D	C	L	A	D	C	L	A	D	C
CD3	1.00	1.00	0.66	1.00	3.00	3.00	2.60	3.00	1.60	1.80	1.60	1.60	1.00	1.00	1.20	1.40
	0.00	0.00	0.47	0.00	0.00	0.00	0.49	0.00	0.49	0.40	0.49	0.49	0.00	0.00	0.75	0.49
CD20	3.00	3.00	3.00	3.20	1.60	1.80	1.20	1.00	1.80	1.80	1.00	1.60	2.00	1.40	0.80	1.00
	0.63	0.00	0.71	0.75	0.49	0.40	0.40	0.00	0.40	0.40	0.63	0.49	0.63	0.80	0.40	0.00
CD79	1.80	2.00	1.25	0.25	1.20	0.80	0.40	0.50	1.60	2.00	1.00	1.00	1.00	0.20	0.00	0.00
	0.40	0.00	0.83	0.43	0.40	0.75	0.49	0.50	0.49	0.00	0.63	0.00	0.89	0.40	0.00	0.00
Iba-1	1.20	1.00	1.00	1.00	3.00	1.80	2.20	2.60	2.00	2.00	1.80	2.00	1.00	1.20	0.60	1.20
	0.40	0.00	0.00	0.00	0.00	0.40	0.75	0.80	0.00	0.00	0.40	0.00	0.63	0.40	0.49	0.75
CD204	0.60	1.00	1.00	0.80	1.20	1.00	1.40	0.80	1.60	1.80	1.60	1.80	0.60	1.00	0.80	0.60
	0.49	0.00	0.00	0.40	0.40	0.63	0.49	0.40	0.49	0.40	0.49	0.40	0.49	0.89	0.40	0.49
m/h antigen	0.80	0.67	1.00	1.00	1.00	1.00	1.40	1.00	2.00	1.80	1.80	1.20	1.20	0.60	0.80	0.80
	0.40	0.47	0.00	0.00	0.63	0.00	0.49	0.00	0.00	0.40	0.40	0.40	0.40	0.80	0.40	0.75
HLA-DR	2.20	1.67	2.00	1.80	2.00	2.60	1.80	2.80	1.80	1.20	1.40	1.80	0.20	0.00	0.40	0.00
	0.75	0.94	1.00	0.98	0.00	0.49	0.40	0.40	0.40	0.40	0.49	0.40	0.40	0.00	0.49	0.00
CD208	0.00	0.00	0.00	0.00	0.20	0.00	0.00	0.00	0.40	0.20	0.40	0.40	0.40	0.20	0.00	0.00
	0.00	0.00	0.00	0.00	0.40	0.00	0.00	0.00	0.49	0.40	0.49	0.49	0.49	0.40	0.00	0.00
CD68	0.00	0.00	0.00	0.20	0.60	0.00	0.00	0.60	0.80	0.80	0.60	0.80	0.20	0.00	0.00	0.00
	0.00	0.00	0.00	0.40	0.49	0.00	0.00	0.49	0.40	0.40	0.49	0.40	0.40	0.00	0.00	0.00

Averages (upper rows) and standard deviations (lower rows) of immunopositive cells were calculated from score values (0, no positive staining cells; 1, < 10%; 2, 10–50%; 3, 51–90%; 4, > 90% of immunolabeled cells) for different compartments of spleen. Thymus tissue was only available from a low number of animals and thus not included in the table. llamas; A, alpacas; D, dromedaries; C, Bactrian camels; PALS, periarteriolar lymphoid sheaths; CD, cluster of differentiation; HLA, human leucocyte antigen; Iba-1, ionized calcium-binding adapter molecule 1; m/h antigen, myeloid/histiocyte antigen.

sinuses, and splenic cords. In a similar manner, immunopositivity was determined for lymphoid nodules (LN), dense nodular lymphoid tissue (DALT), and diffuse lymphoid tissue (DLT) of lymph nodes, and medulla and cortex of thymus according to the following score: 0 = no positive staining cells; 1 = < 10%; 2 = 10–50%; 3 = 51–90%; 4 = >90% immunolabeled cells.

3. Results and discussion

3.1. Histopathology

Even though lymphoid organs with significant lesions were avoided in the present study, intestinal diseases and associated lesions in tributary lymph nodes of camels are rather common

immunopositive cells are characterized by lymphocyte morphology and an intense membrane-bound signal. Most cells have relatively low amount of cytoplasm, suggestive of mature B cells. However, there are scattered cells with a relatively larger morphology, suggestive of immunoblasts. Scale bar = 20 μ m. (E) CD79 α ; spleen. Compared to CD20 (A) only few scattered cells, immunopositive for CD79 α are seen within the MC, PALS, and RP of the spleen, while there is a relatively intense background staining and diffuse immunopositivity in blood vessel walls (arrow). Scale bar = 100 μ m. (F) CD79 α ; lymph node. CD79 α antigen is mainly expressed in LN of lymph nodes. Moderate numbers of scattered immunopositive cells are also found throughout the DLT, while there are only rarely CD79 α positive cells within the DALT. Similar to spleen, blood vessel walls stain also positive (arrows). Scale bar = 100 μ m. (G) CD79 α ; thymus. Few cells, predominantly located within the thymus medulla stain positive for CD79 α antigen. Scale bar = 100 μ m. (H) CD79 α ; lymph node. Higher magnification of the inset in (F). Morphologically, CD79 α immunopositive cells are characterized by lymphocyte morphology with a cytoplasmic immunoreaction pattern. However, few cells show a nuclear staining pattern, which is considered a false positive reaction (arrowheads). Scale bar = 20 μ m.

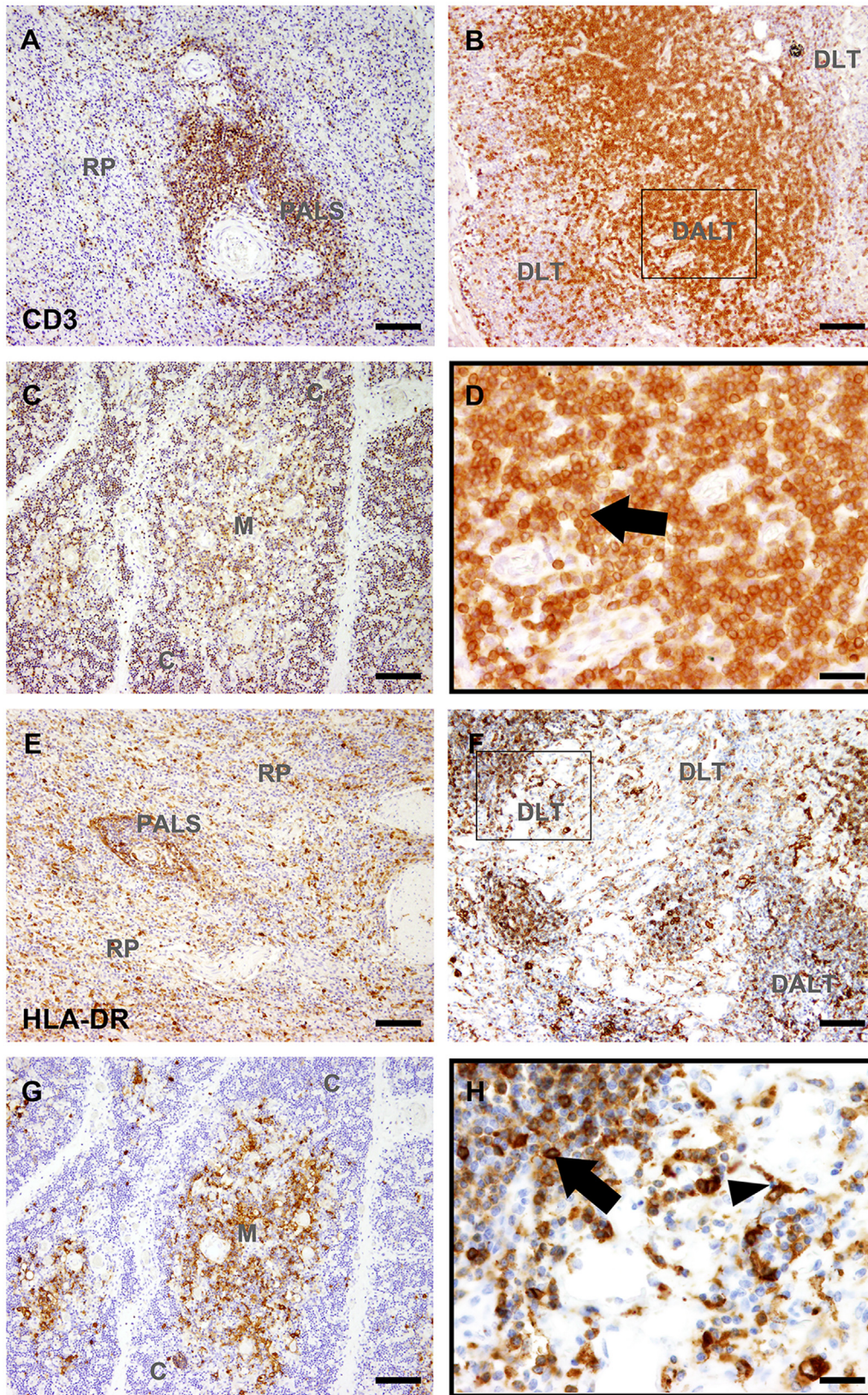


Fig. 2. Representative immunohistochemical reactions for detection of T cells and antigen presenting cells in the spleen, lymph node, and thymus of a Bactrian camel (A–D: CD3; E–H: HLA-DR). Avidin-biotin-peroxidase complex method with 3,3'-diaminobenzidine as chromogen. (A) CD3; spleen. CD3 positive cells are predominantly seen throughout the periarteriolar lymphoid sheath (PALS), while only scattered immunopositive cells are seen throughout the red pulp (RP). Scale bar = 100 μ m. (B) CD3; lymph node. Numerous cells stain positive for CD3 antigen within dense anodular lymphoid tissue (DALT), which resembles the T cell compartment of camelids. Moderate numbers of scattered immunopositive cells are also noted within diffuse lymphoid tissue (DLT). Scale bar = 100 μ m. (C) CD3; thymus. Numerous CD3-positive cells are seen within the medulla (M) and cortex (C) of thymus. Scale bar = 100 μ m. (D) CD3; lymph node. Higher magnification of the inset in (B). Morphologically, CD3 immunopositive cells are characterized by lymphocyte morphology with intense membrane-bound signal (arrow). Scale bar = 20 μ m. (E) HLA-DR; spleen. Numerous HLA-DR positive cells are located

Table 3
Distribution of antigens in different compartments of lymph nodes.

Detected antigen	Lymphoid nodules								Dense anodular lymphoid tissue								Diffuse lymphoid tissue							
	L	L	A	A	D	D	C	C	L	L	A	A	D	D	C	C	L	L	A	A	D	D	C	C
CD3	1.00 0.00	1.00 0.00	1.00 0.00	1.00 0.00	1.20 0.40	1.20 0.75	1.25 0.43	1.20 0.40	2.80 0.40	3.00 0.00	2.80 0.40	2.60 0.49	2.80 0.40	2.60 0.49	3.00 0.00	3.00 0.00	1.20 0.40	0.80 0.40	1.00 0.00	1.40 0.49	1.00 0.63	0.80 0.40	1.00 0.00	1.00 0.00
CD20	3.20 0.40	3.00 0.00	2.80 0.40	2.75 0.43	3.00 0.00	3.00 0.63	3.40 0.49	2.80 0.75	1.60 0.49	1.60 0.80	2.00 0.63	1.60 0.80	1.60 0.49	1.40 0.49	1.60 0.49	2.00 0.63	1.20 0.40	1.80 0.98	1.80 0.40	0.80 0.40	1.20 0.40	2.40 0.49	1.40 0.49	
CD79	2.80 0.40	2.75 0.43	1.00 0.63	1.80 0.40	1.50 0.87	1.40 1.02	1.80 0.98	1.60 1.36	2.00 0.00	1.80 0.40	1.60 0.49	2.00 0.00	1.25 0.43	1.20 0.40	1.20 0.75	2.20 0.75	1.80 0.40	0.40 0.49	1.00 0.89	1.25 0.43	0.80 0.40	1.00 0.63	0.60 0.49	
Iba-1	1.60 0.49	1.75 0.43	1.00 0.63	1.20 0.40	1.00 0.00	1.20 0.40	1.20 0.40	1.20 0.40	2.00 0.00	1.60 0.49	1.40 0.80	1.80 0.40	1.20 0.40	1.80 0.40	1.60 0.49	3.00 0.00	2.40 0.49	2.00 0.63	2.40 0.49	2.20 0.75	2.00 0.63	2.00 0.63	2.80 0.40	
CD204	1.00 0.00	1.25 0.43	1.00 0.00	1.00 0.63	0.80 0.40	0.60 0.49	1.00 0.00	0.60 0.49	1.40 0.49	1.40 0.80	1.20 0.40	1.20 0.40	1.20 0.40	0.80 0.00	1.00 0.40	1.20 0.40	2.20 0.40	1.80 0.40	2.00 0.00	2.40 0.49	2.20 0.75	2.00 0.63	1.60 0.49	2.00 0.00
m/h antigen	1.20 0.40	0.75 0.43	0.80 0.40	0.40 0.49	0.80 0.40	0.60 0.49	1.00 0.00	0.80 0.40	1.00 0.00	0.80 0.40	0.80 0.40	0.60 0.49	0.80 0.40	1.00 0.00	1.40 0.80	1.00 0.00	1.80 0.40	1.60 0.49	1.20 0.40	1.40 0.49	1.40 0.80	1.40 0.49	1.40 0.49	1.80 0.75
HLA-DR	2.60 0.49	2.75 0.43	2.60 0.80	2.20 0.98	2.40 0.80	2.60 0.80	2.20 0.75	3.00 0.00	2.20 0.40	1.60 0.49	2.00 0.00	2.00 0.00	1.60 0.49	1.80 0.40	1.80 0.40	1.80 0.40	1.60 0.49	2.00 0.63	2.00 0.63	2.20 0.40	1.60 0.49	1.60 0.49	2.20 0.40	1.40 0.49
CD208	0.20 0.40	0.00 0.00	0.00 0.00	0.00 0.00	0.00 0.00	0.00 0.00	0.00 0.00	0.00 0.00	0.60 0.49	0.80 0.40	0.20 0.40	0.40 0.49	0.40 0.49	0.00 0.00	0.20 0.40	0.20 0.40	1.00 0.00	0.20 0.40	0.40 0.80	0.40 0.49	0.60 0.49	0.60 0.49	0.40 0.49	0.60 0.49
CD68	0.20 0.40	0.00 0.00	0.00 0.00	0.00 0.00	0.00 0.00	0.00 0.00	0.20 0.40	0.20 0.40	0.60 0.49	0.60 0.49	0.20 0.40	0.40 0.49	0.20 0.40	0.20 0.40	0.60 0.49	0.40 0.40	0.80 0.40	0.80 0.00	0.00 0.00	0.20 0.40	0.20 0.40	0.60 0.49	0.40 0.49	0.40 0.49

Averages (upper rows) and standard deviations (lower rows) of immunopositive cells were calculated from score values (0, no positive staining cells; 1, <10%; 2, 10–50%; 3, 51–90%; 4, >90% of immunolabeled cells) for different compartments of pulmonary (white values) and mesenteric lymph nodes (grey values). Thymus tissue was only available from a low number of animals and thus not included in the table. llamas; A, alpacas; D, dromedaries; C, Bactrian camels; CD, cluster of differentiation; HLA, human leucocyte antigen; Iba-1, ionized calcium-binding adapter molecule 1; m/h antigen, myeloid/histiocyte antigen.

(Bekele, 2002; Hussein et al., 1987; Theuß et al., 2014). Consequently, evaluation of H&E staining of lymphoid tissues by light microscopy revealed minor lesions in the majority of the investigated lymphoid organs. These lesions included mild to moderate degrees of extramedullary hematopoiesis, hyperemia, hemosiderosis, sinus histiocytosis, plasmocytosis, focal fibrosis, edema, multifocal hemorrhages, and mild neutrophilic and eosinophilic infiltrations.

3.2. Immunohistochemistry

In the present study, six out of ten mc antibodies and three out of four pc antibodies were demonstrated to be suitable for detection of different antigens, based on an expected immunoreactivity distribution pattern and cellular morphology in lymphoid tissues of camelids. Immunohistochemistry was only judged specific if cellular staining characteristics fitted the pattern in canine and bovine control tissue (Supplemental Fig. S1 in the online version at DOI: 10.1016/j.vetimm.2017.01.001) and if negative controls of camelid tissue (Supplemental Fig. S2 in the online version at DOI: 10.1016/j.vetimm.2017.01.001) lacked immunoreactivity. Averages and standard deviations of the semiquantitative scores for all nine antigens are summarized in Tables 2 and 3 with respect to different compartments of spleen and lymph node tissues, respectively. Four mc antibodies for the detection of Pax-5- (B cells), MUM1- (plasma cells, certain B cells), Foxp3- (regulatory T cells), and CD205-antigen (dendritic cells (DCs), certain B and T cells) and one pc antibody for identification of lysozyme (macrophages) showed specific reaction patterns on canine and bovine positive controls, respectively, but lacked specific immunopositivity on FFPE sections of camelid

organs in all tested dilutions (Supplemental Fig. S3 in the online version at DOI: 10.1016/j.vetimm.2017.01.001) without and with both tested pretreatments (heat retrieval and pronase treatment, respectively). Contrary to the present investigation, Pax-5 has been reported to react on GALT of alpacas (Steffen et al., 2014); however, it remains unclear if a similar or a differing antibody has been used in the former study or whether the contrasting results are attributed to variations in the protocols used. No major differences were determined between different camelid species concerning the cellular staining patterns and the general distribution of immunolabeled cells for all investigated antibodies (Tables 2 and 3). Thus, the results implicate a relatively similar anatomical architecture of lymphoid organs of different camelid species, even if detailed anatomical descriptions of these organs for llamas, alpacas and Bactrian camels are not available. Moreover, no considerable differences were discovered between tracheobronchial and mesenteric lymph nodes in any species.

3.3. B cells

Two out of three different antibodies appeared suitable to label cells of the B cell lineage (Table 1). In spleen, CD20 immunoreactive cells were mainly located in small follicles adjacent to the PALS (Malpighian corpuscles, Fig. 1A). Similarly, tracheobronchial and mesenteric lymph nodes showed positive immunostaining within LN and adjacent areas of DALT and DLT (Fig. 1B). Scattered immunoreactive cells were additionally present in all other investigated compartments of spleen and lymph nodes. In thymus, CD20-positive cells were mainly located in the medulla (score ½; Fig. 1C). Single positive cells were additionally detected mul-

throughout the splenic RP and are similarly found within the PALS. Scale bar = 100 µm. (F) HLA-DR, lymph node. Immunoreactive cells are seen predominantly seen within the DLT; however, moderate numbers of cells within the DALT are similarly immunoreactive. (G) HLA-DR, thymus. HLA-DR positive cells are mainly located within the thymus medulla. Fewer cells throughout, scattered throughout the cortex are also HLA-DR positive. Scale bar = 100 µm. (H) HLA-DR, lymph node. Higher magnification of the inset in (E). Morphologically, the anti-HLA-DR antibody labels cells with histiocyte-like morphology and produces an intense membranous and intracytoplasmic diffuse positive signal on medium sized to large cells with plenty cytoplasm and cytoplasmic extensions (arrowhead). In addition, cells with lymphocyte morphology and lower amounts of cytoplasm are similarly positive for HLA-DR (arrow). Scale bar = 20 µm.

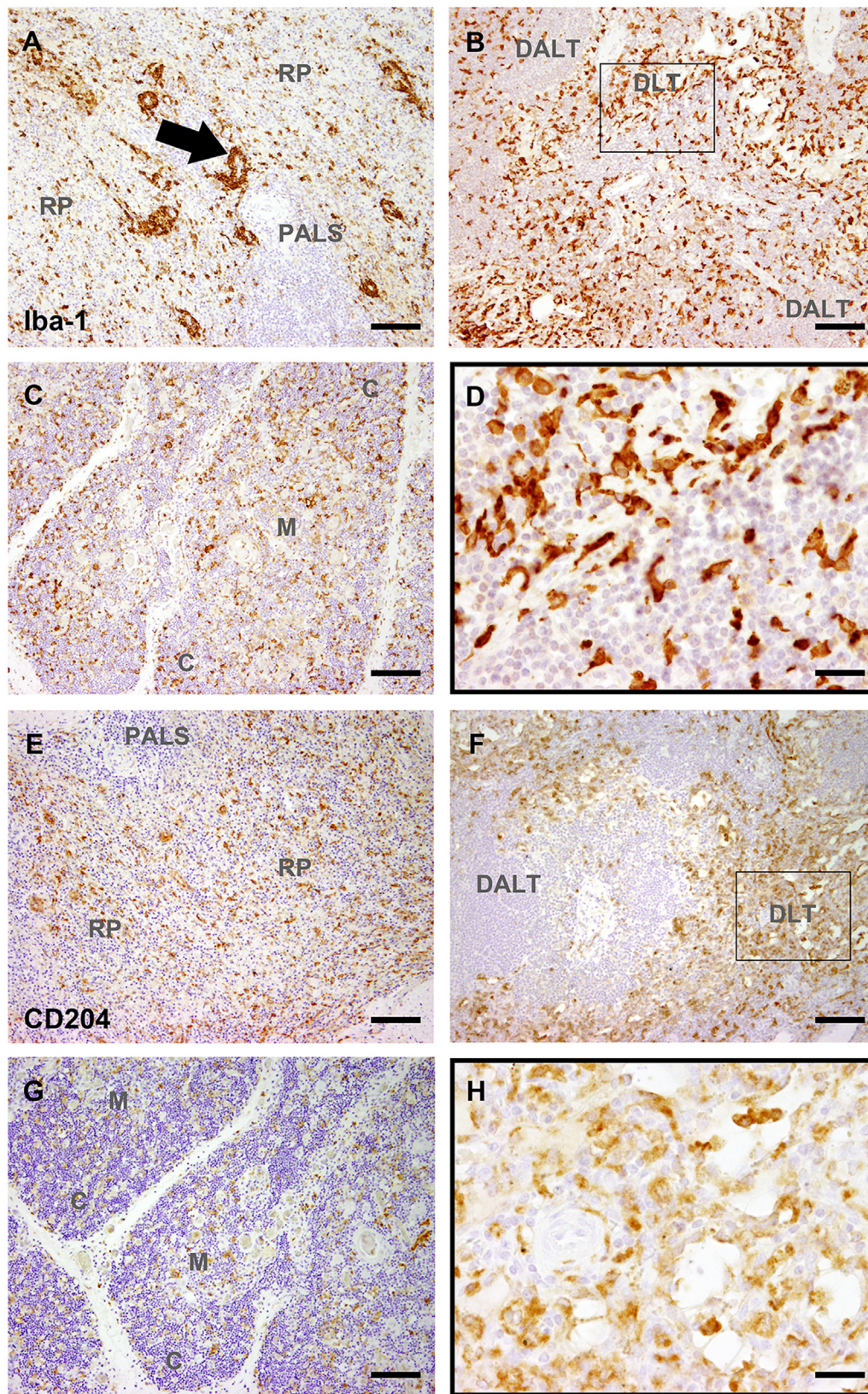


Fig. 3. Representative immunohistochemical reactions for detection of histiocytic cells in the spleen, lymph node, and thymus of a Bactrian camel (A–D: Iba-1; E–H: CD204). Avidin-biotin-peroxidase complex method with 3,3'-diaminobenzidine as chromogen. (A) Iba-1; spleen. Iba-1-specific immunohistochemistry shows a characteristic perivascular staining pattern (arrow), which is not observed for any other marker. Several immunopositive cells are also noted scattered throughout the splenic red pulp (RP), and perivascularly within the periarteriolar lymphoid sheath (PALS). Scale bar = 100 μ m. (B) Iba-1; lymph node. Numerous cells stain positive for Iba-1 antigen within diffuse lymphoid tissue (DLT), which resembles the T cell compartment of camelids. Moderate numbers of scattered immunopositive cells are also noted within dense anodular lymphoid tissue (DALT). Scale bar = 100 μ m. (C) Iba-1; thymus. A moderate number staining intensely positive for Iba-1 antigen are seen within both compartments of the thymus, cortex (C) and medulla (M). Scale bar = 100 μ m. (D) Iba-1; lymph node. Higher magnification of the inset in (B). Morphologically, Iba-1 immunopositive cells

tifocally within the cortex. CD20 immunoreactive cells showed a distinct membrane-bound immunopositivity and were characterized by small size, round shape, scant amounts of cytoplasm and a centrally located round nucleus resembling mature B cells. Additionally, larger cells with similar morphology but a higher amount of cytoplasm were detected within germinal centers, thus most likely representing immunoblasts (Fig. 1D). These observations are in consistence with findings of previous studies on frozen dromedary tissue, which described relatively similar localization of the B cell specific antigens CD21 and CD22 (Zidan and Pabst, 2004, 2012; Zidan et al., 2000b). In humans, CD20 is mainly expressed by pre- and mature B cells; however, some human T cell subsets have also been reported to be immunoreactive for CD20 (Hultin et al., 1993). Interestingly, the present results suggest that a similar expression pattern might exist in camelids, as CD20 was expressed by some lymphocytes within the DALT, which resembles the T cell compartment of camelid lymph nodes (Abdel-Magied et al., 2001; Zidan and Pabst, 2012). The distribution and amount of CD20 positive cells in camelid thymus are in line with investigations on human thymus, which detected similar numbers of B cells in the medulla of children (Spencer et al., 1992). B cells have been reported to present autoantigens as an important step in the negative selection of T lymphocytes and induction of T cell tolerance (Rother et al., 2016).

Similarly to CD20, CD79 α labeled cells were predominantly located in splenic follicles (Fig. 1E), LN (Fig. 1F), and thymic medulla (Fig. 1G). However, scattered positive cells were inconsistently present in all other compartments, including DLT of lymph nodes (Fig. 1F), and distinct staining was rare in splenic follicles, which however stained positive for CD20 (Fig. 1A). Overall, the CD79 α labeled cell population was considerably smaller compared to CD20, indicating that CD20 might label a broader population of the B cell lineage. Moreover, the anti-CD79 α antibody produced pronounced unspecific background and a positive immunoreactivity of non-lymphoid cells including smooth muscle and endothelium as previously mentioned for porcine tissue (Chianini et al., 2001; Fig. 1E). A nuclear staining pattern for CD79 α is known to represent an unspecific reaction in several species including dogs and cats (Raskin, 2016), thus only a distinct cytoplasmic and membranous staining was judged as specific immunoreactivity (Fig. 1H).

3.4. T cells

One out of two tested antibodies detected T cells in camelids (Table 1). As previously reported for frozen sections of dromedaries (Zidan and Pabst, 2012; Zidan et al., 2000b), CD3 positively staining cells were mainly located within the PALS of spleen (Fig. 2A) and the DALT of lymph nodes (Fig. 2B). The DALT of dromedaries resembles the T cell compartment and is comparable to the paracortex of other mammalian species (Abdel-Magied et al., 2001). A minor population of CD3-immunoreactive cells was dispersed within cords and sinuses of the red pulp and single cells were detected in the splenic follicles as well as in LN and DLT of lymph nodes (Fig. 2A and B). Additionally, abundant numbers of CD3-positive cells were present in the medulla and cortex of thymus as expected (score 3; Fig. 2C). Whereas cortically located cells were closely packed, positive cells within the medulla were more loosely arranged and intermingled with immunonegative cells. In all locations, the pc anti-CD3 antibody displayed a distinct membrane-bound signal on

cells with lymphoid morphology (Fig. 2D). Similarly to CD20 and CD79 α , commercially available anti-CD3 antibodies have been frequently used in other cross-reactivity studies and are known to be suitable for various species (Beineke et al., 2001; Chianini et al., 2001; Heinrich et al., 2015; Vidana et al., 2014).

3.5. Histiocytic cells

Six out of eight markers labeled subsets of camelid histiocytic cells (Table 1). The histiocytic lineage includes an extensive range of phenotypes and a variety of heterogeneous subsets, thus requiring several markers for their identification (Rehg et al., 2012). The morphology of labeled cells was relatively similar for all markers mentioned below. There was membranous and intracytoplasmic diffuse positivity on medium sized to large cells with plenty cytoplasm, kidney-shaped nuclei, and more or less distinct, cytoplasmic extensions. The most widespread immunoreaction pattern was observed by detection of HLA-DR (α chain). The anti-HLA-DR antibody labeled the cytoplasm of a large population of macrophage-like cells. Most of these cells were located in the splenic red pulp (Fig. 2E), the DLT of lymph nodes (Fig. 2F), and the medulla of thymus (Fig. 2G). Additionally, moderate numbers of HLA-DR-positive cells were observed in T cell compartments of spleen and lymph nodes, germinal centers of splenic follicles, LN of lymph nodes, and the cortex of thymus (Fig. 2E–G). Nonetheless, HLA-DR was also expressed by a cell population of moderate size with lymphoid morphology (Fig. 2H) in splenic follicles, LN, PALS, DALT, and thymus (score 3). These findings are consistent with previously described distribution patterns of HLA-DR in humans (Daar et al., 1984), dogs (Vilafranca et al., 1995; Wünschmann et al., 2000), and cattle (Romero-Palomo et al., 2013). In contrast to some other macrophage markers mentioned below, HLA-DR antigen is also apparent on DCs, B cells, activated T cells, and certain endothelia and therefore seems relatively inappropriate for labelling of a specific histiocytic lineage (Daar et al., 1984). The results indicate that the same might be true for camelid tissue.

Overall, the applied antibodies against Iba-1 (Fig. 3A–D), CD204 (Fig. 3E–H), and myeloid/histiocyte antigen (Fig. 4A–D) stained a relatively lower proportion of cells as compared to anti-HLA-DR specific IHC, thus probably indicating higher specificity. All three antibodies labeled macrophage-like cells in the splenic red pulp and DLT of lymph nodes. Fewer cells were localized in splenic follicles, LN and DALT. Surprisingly, Iba-1-specific IHC revealed an additional characteristic circular staining pattern, surrounding smaller blood vessels and central arteries of the splenic PALS of all camelid species (Fig. 3A). In contrast to myeloid/histiocyte antigen and CD204, which were expressed to a low degree in medulla and cortex of thymus (score 1; Figs. 3G, 4C), Iba-1 antigen was expressed to a moderate degree (score 2) in both compartments (Fig. 3C). According to the literature, Iba-1 is located on all cell types of the monocyte/macrophage lineage of mice (Köhler, 2007) and dogs (Pierezan et al., 2014), and CD204 is known to be expressed by red pulp and sinus macrophages of several species (Tomokiyo et al., 2002). Myeloid/histiocyte antigen (synonym leucocyte antigen L1; calprotectin) is widely expressed by recently infiltrated, blood-borne monocytes/macrophages of humans, monkeys, dogs, and in bovine granulomas (Fernandez et al., 2017; Poston and Hussain, 1993; Soulas et al., 2011; Spitzbarth et al., 2011). Moreover, myeloid/histiocyte antigen specific antibodies

are characterized by histiocyte-like morphology with abundant intensely and diffusely labeled cytoplasm and many cells show pronounced cytoplasmic projections. Scale bar = 20 μ m. (E) CD204; spleen. Similar to Iba-1 but with absent perivascular staining pattern, several immunopositive cells are noted throughout the splenic RP with few immunoreactive cells in the PALS. Scale bar = 100 μ m. (F) CD204; lymph node. CD204 immunopositive cells are mainly found within the DLT, while only few scattered cells are positive within the DALT. Scale bar = 100 μ m. (G) CD204, thymus. In contrast to Iba-1 (C), a relatively lower number of CD204 immunopositive cells is noted within thymus medulla and cortex. Scale bar = 100 μ m. (H) CD204; lymph node. Higher magnification of the inset in (F). CD204 positive cells are characterized by relatively high amounts of diffusely stained cytoplasm, peripheral nuclei, and histiocyte-like morphology. Scale bar = 20 μ m.

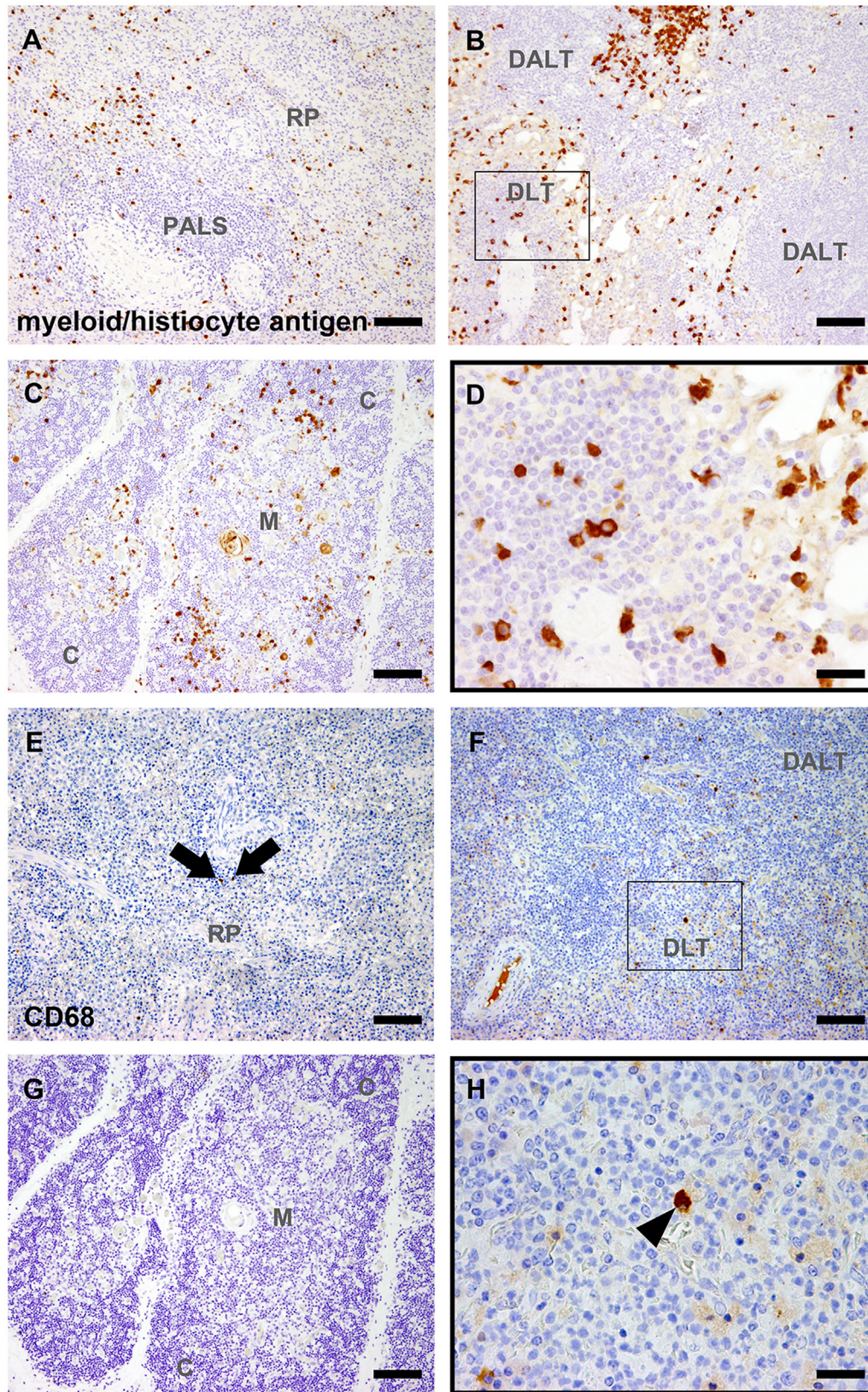


Fig. 4. Representative immunohistochemical reactions for detection of histiocytic cells in the spleen, lymph node, and thymus of a Bactrian camel (A–D: myeloid/histiocyte antigen; E–H: CD68). Avidin-biotin-peroxidase complex method with 3,3'-diaminobenzidine as chromogen. (A) Myeloid/histiocyte antigen; spleen. Several intensely immunopositive cells are observed scattered throughout the splenic red pulp (RP) and within the periarteriolar lymphoid sheath (PALS). Scale bar = 100 μ m. (B) Myeloid/histiocyte antigen; lymph node. Positively labeled cells are mainly seen within diffuse lymphoid tissue (DLT) with fewer numbers of scattered immunopositive cells within dense anodular lymphoid tissue (DALT). Note the cluster of immunopositive cells within the sinus and DLT in the upper part of the figure. Scale bar = 100 μ m. (C) Myeloid/histiocyte antigen; thymus. Scattered immunopositive cells are seen throughout the cortex (C) and medulla (M) of the thymus. Scale bar = 100 μ m. (D) Myeloid/histiocyte antigen; lymph node. Higher magnification of the inset in (B). Morphologically, the cells reacting positive for myeloid/histiocyte antigen are characterized

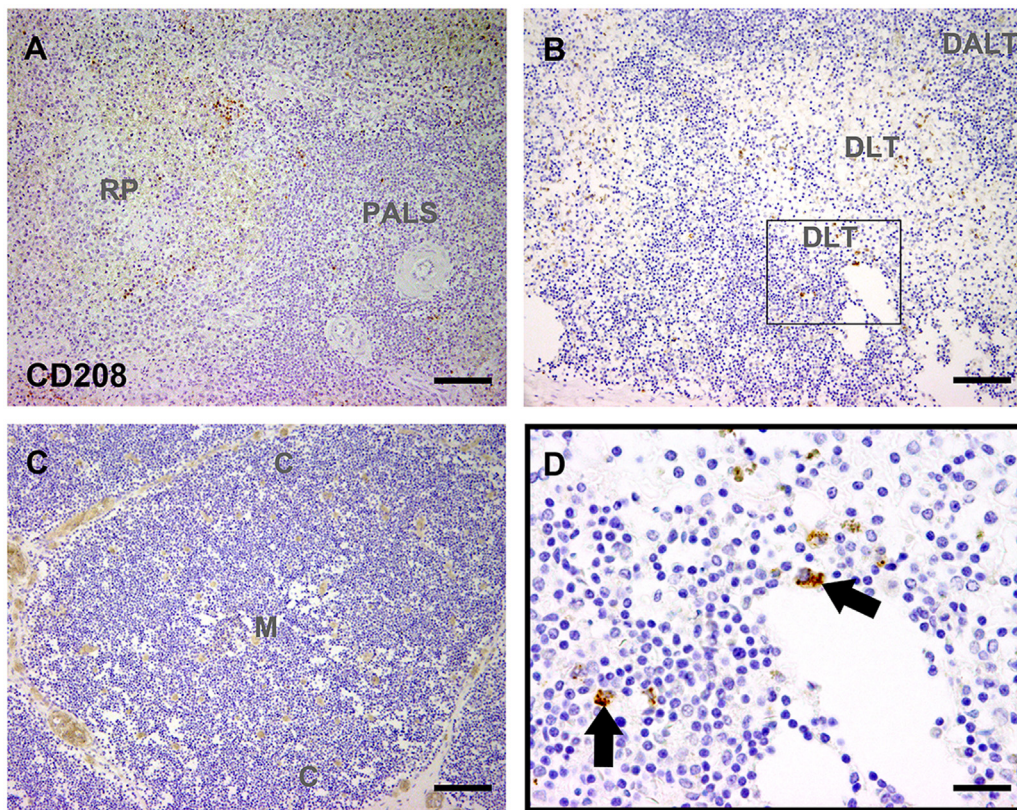


Fig. 5. Representative immunohistochemical reaction for the detection of dendritic cells in the spleen, lymph node, and thymus of a Bactrian camel (A–D: CD208). Avidin-biotin-peroxidase complex method with 3,3'-diaminobenzidine as chromogen. (A) CD208; spleen. Immunopositive cells are noted scattered throughout the splenic red pulp (RP) and rarely within the periarteriolar lymphoid sheath (PALS). Scale bar = 100 μ m. (B) CD208; lymph node. Similar to the spleen, few individualized CD208 positive cells are seen in all lymph node compartments (DLT = diffuse lymphoid tissue; DALT = dense anodular lymphoid tissue). Scale bar = 100 μ m. (C) CD208; thymus. Note absent immunopositivity. Scale bar = 100 μ m. (D) CD208; lymph node. Higher magnification of the inset in (B). CD208 immunopositive cells are characterized by peripherally located nuclei, moderate to high amounts of cytoplasm, and an intense coarsely granular immunosignal within the cytoplasm (arrows). The granular signal indicates that the signal is associated with lysosomes of dendritic cells (CD208 = synonym for dendritic cell lysosomal-associated membrane protein [DC-LAMP]). Scale bar = 20 μ m.

are also suitable for labelling of neutrophils in contrast to all previously mentioned markers (Brandtzaeg et al., 1992; Flavell et al., 1987). In line with these investigations, some cells with neutrophilic morphology were similarly labeled in the tracheo-bronchial and mesenteric lymph nodes of llamas, dromedaries and Bactrian camels with mild neutrophilic infiltration (Supplemental Fig. S4 in the online version at DOI: [10.1016/j.vetimm.2017.01.001](https://doi.org/10.1016/j.vetimm.2017.01.001)).

CD68-specific IHC stained the cytoplasm of only very few cells in spleen and lymph nodes of camels in the present study regardless of the species (Fig. 4E–H). They were mainly located in splenic cords of the red pulp (Fig. 4E), and DALT and DLT of lymph nodes (Fig. 4F). CD68 was not expressed in thymus of any species (Fig. 4G). Morphologically, positive cells showed histiocytic morphology with abundant diffusely to slightly granular positive cytoplasm and peripheral nuclei (Fig. 4H). In contrast to the sparse distribution in camelids, CD68, a lysosomal/plasma membrane shuttling protein localized to endo- and lysosomes, is known to be a pan-macrophage marker in humans (Holness and Simmons, 1993; Taylor et al., 2005). Further studies will be needed to evaluate how the CD68-positive camelid population differs from the rather broader positive population in other species, and whether the observed differences are attributed to the species or technical variations.

Antibodies against CD205 and CD208 antigen were applied for the detection of DCs, as previously reported in cattle (Romero-Palomo et al., 2013), sheep (Åkesson et al., 2008) and humans (de Saint-Vis et al., 1998; Geijtenbeek et al., 2000). Only CD208 (synonym dendritic cell lysosomal-associated membrane protein [DC-LAMP]) revealed specific immunoreaction on few histiocytic cells in camelid tissue (Fig. 5A–D). Positive cells were rarely present in the splenic red pulp and PALS (Fig. 5A) as well as in LN, DALT, and the DLT of lymph nodes (Fig. 5B), while CD208 was neither detected in the medulla nor the cortex of thymus (Fig. 5C). Morphologically, positive camelid cells were characterized by an intense coarsely granular immunosignal within the cytoplasm, probably indicating labelling of lysosomes (Fig. 5D). CD208 is reported to be expressed by mature and activated DCs, but not on unactivated DCs of humans (de Saint-Vis et al., 1998). The relative paucity of positive cells on camelid tissue indicates that CD208 might similarly detect only mature camelid DCs.

4. Conclusion

Summarized, 9 out of 14 tested commercially available antibodies showed immunoreactivity on distinct cell types in FFPE

by histiocytic morphology, moderate size, round to oval cell bodies and abundant cytoplasm, which is intensely and diffusely positive. Some cells show discrete cellular processes. Scale bar = 20 μ m. (E) CD68; spleen. Only very few individualized cells (arrows) within the splenic RP are immunoreactive for CD68, while there are no positive cells within the PALS. Scale bar = 100 μ m. (F) CD68; lymph node. Similar to spleen, CD68 is only rarely expressed on very few cells within DLT and DALT. Scale bar = 100 μ m. (G) CD68; thymus. No immunopositive cells are seen in the thymus cortex and medulla. Scale bar = 100 μ m. (H) CD68; lymph node. Higher magnification of the inset in (F). Morphologically, CD68 positive cells show histiocytic morphology with abundant diffusely to slightly granular positive cytoplasm and peripheral nuclei (arrowhead). Scale bar = 20 μ m.

lymphoid tissue of different camelid species. The presented antibody panel appears to be suitable for the detection of the most important subpopulations of immune cells, including T and B cells, macrophages and DCs in FFPE tissue of camelids. Doubtlessly, the present results, especially those obtained from thymus, need to be interpreted on the basis of relatively small animal numbers. Nevertheless, the established markers will provide a solid basis for the investigation of naturally occurring and experimental diseases of camelids with a special emphasis on emerging spill-over infections such as Middle East respiratory syndrome.

Acknowledgements

The authors would like to thank Bettina Buck, Petra Grünig, Kerstin Schöne, Caroline Schütz, Danuta Waschke, and Nicole Lenort for excellent technical assistance. This research was performed as part of the Zoonoses Anticipation and Preparedness Initiative (ZAPI project; IMI Grant Agreement no. 115760), with the assistance and financial support of IMI and the European Commission, and in-kind contributions from EFPIA partners.

References

Åkesson, C.P., McL Press, C., Espenes, A., Aleksandersen, M., 2008. Phenotypic characterisation of intestinal dendritic cells in sheep. *Dev. Comp. Immunol.* 32, 837–849.

Abdel-Magied, E.M., Taha, A.A., al-Qarawi, A.A., Elfaki, M.G., 2001. The parotid, mandibular and lateral retropharyngeal lymph nodes of the camel (*Camelus dromedarius*). *Anat. Histol. Embryol.* 30, 199–203.

Ackermann, M.R., DeBey, B.M., Stabel, T.J., Gold, J.H., Register, K.B., Meehan, J.T., 1994. Distribution of anti-CD68 (EBM11) immunoreactivity in formalin-fixed, paraffin-embedded bovine tissues. *Vet. Pathol.* 31, 340–348.

Adney, D.R., van Doremalen, N., Brown, V.R., Bushmaker, T., Scott, D., de Wit, E., Bowen, R.A., Munster, V.J., 2014. Replication and shedding of MERS-CoV in upper respiratory tract of inoculated dromedary camels. *Emerg. Infect. Dis.* 20, 1999–2005.

Alldinger, S., Wünschmann, A., Baumgärtner, W., Voss, C., Kremmer, E., 1996. Up-regulation of major histocompatibility complex class II antigen expression in the central nervous system of dogs with spontaneous canine distemper virus encephalitis. *Acta Neuropathol.* 92, 273–280.

Beineke, A., Siebert, U., Wünschmann, A., Stott, J.L., Prengel, I., Kremmer, E., Baumgärtner, W., 2001. Immunohistochemical investigation of the cross-reactivity of selected cell markers from various species for characterization of lymphatic tissues in the harbour porpoise (*Phocoena phocoena*). *J. Comp. Pathol.* 125, 311–317.

Bekele, T., 2002. Epidemiological studies on gastrointestinal helminths of dromedary (*Camelus dromedarius*) in semi-arid lands of eastern Ethiopia. *Vet. Parasitol.* 105, 139–152.

Brandtzaeg, P., Dale, I., Gabrielsen, T.O., 1992. The leucocyte protein L1 (calprotectin): usefulness as an immunohistochemical marker antigen and putative biological function. *Histopathology* 21, 191–196.

Burger, P.A., 2016. The history of Old World camelids in the light of molecular genetics. *Trop. Anim. Health Prod.* 48, 905–913.

Chan, J.F., Lau, S.K., To, K.K., Cheng, V.C., Woo, P.C., Yuen, K.Y., 2015. Middle East respiratory syndrome coronavirus: another zoonotic betacoronavirus causing SARS-like disease. *Clin. Microbiol. Rev.* 28, 465–522.

Chianini, F., Majo, N., Segales, J., Dominguez, J., Domingo, M., 2001. Immunohistological study of the immune system cells in paraffin-embedded tissues of conventional pigs. *Vet. Immunol. Immunopathol.* 82, 245–255.

Daar, A.S., Fuggle, S.V., Fabre, J.W., Ting, A., Morris, P.J., 1984. The detailed distribution of MHC Class II antigens in normal human organs. *Transplantation* 38, 293–298.

Duraiyan, J., Govindarajan, R., Kaliyappan, K., Palanisamy, M., 2012. Applications of immunohistochemistry. *J. Pharm. Bioallied Sci.* 4, S307–S309.

Faldyna, M., Samankova, P., Leva, L., Cerny, J., Oujezdska, J., Rehakova, Z., Sinkora, J., 2007. Cross-reactive anti-human monoclonal antibodies as a tool for B-cell identification in dogs and pigs. *Vet. Immunol. Immunopathol.* 119, 56–62.

Feng, Y., Wang, W., Guo, J., Li, Y., Yang, G., Su, N., Zhang, L., Xu, W., Sheng, Z., Ma, L., Gui, J., Lin, H., Tu, C., 2014. Disease outbreaks caused by steppe-type rabies viruses in China. *Epidemiol. Infect.* 143, 1287–1291.

Fernandez, M., Benavides, J., Castano, P., Elguezabal, N., Fuertes, M., Munoz, M., Royo, M., Ferreras, M.C., Perez, V., 2017. Macrophage subsets within granulomatous intestinal lesions in Bovine paratuberculosis. *Vet. Pathol.* 54, 82–93. <http://dx.doi.org/10.1177/0300985816653794>.

Flavell, D.J., Jones, D.B., Wright, D.H., 1987. Identification of tissue histiocytes on paraffin sections by a new monoclonal antibody. *J. Histochem. Cytochem.* 35, 1217–1226.

Geijtenbeek, T.B.H., Torensma, R., van Vliet, S.J., van Duijnhoven, G.C.F., Adema, G.J., van Kooyk, Y., Figdor, C.G., 2000. Identification of DC-SIGN, a novel dendritic

cell-specific ICAM-3 receptor that supports primary immune responses. *Cell* 100, 575–585.

Haagmans, B.L., van den Brand, J.M.A., Raj, V.S., Volz, A., Wohlsein, P., Smits, S.L., Schipper, D., Bestebroer, T.M., Okba, N., Fux, R., Bensaïd, A., Solanes Foz, D., Kuiken, T., Baumgärtner, W., Segalés, J., Sutter, G., Osterhaus, A.D.M.E., 2015. An orthopoxvirus-based vaccine reduces virus excretion after MERS-CoV infection in dromedary camels. *Science* 351, 77–81.

Heinrich, F., Jungwirth, N., Carlson, R., Tipold, A., Boer, M., Scheibe, T., Molnar, V., von Dornberg, K., Spitzbarth, I., Puff, C., Wohlsein, P., Baumgärtner, W., 2015. Immunophenotyping of immune cell populations in the raccoon (*Procyon lotor*). *Vet. Immunol. Immunopathol.* 168, 140–146.

Holness, C.L., Simmons, D.L., 1993. Molecular cloning of CD68, a human macrophage marker related to lysosomal glycoproteins. *Blood* 81, 1607–1613.

Hultin, L.E., Hausner, M.A., Hultin, P.M., Giorgi, J.V., 1993. CD20 (pan-B cell) antigen is expressed at a low level on a subpopulation of human T lymphocytes. *Cytometry* 14, 196–204.

Hussein, H.S., Kasim, A.A., Shawa, Y.R., 1987. The prevalence and pathology of Eimeria infections in camels in Saudi Arabia. *J. Comp. Pathol.* 97, 293–297.

Joseph, S., Wernery, U., Teng, J.L., Wernery, R., Huang, Y., Patteril, N.A., Chan, K.H., Elizabeth, S.K., Fan, R.Y., Lau, S.K., Kinne, J., Woo, P.C., 2016. First isolation of West Nile virus from a dromedary camel. *Emerg. Microbes Infect.* 5, e53.

Köhler, C., 2007. Allograft inflammatory factor-1/lonized calcium-binding adapter molecule 1 is specifically expressed by most subpopulations of macrophages and spermatids in testis. *Cell Tissue Res.* 330, 291–302.

Kato, Y., Murakami, M., Hoshino, Y., Mori, T., Maruo, K., Hirata, A., Nakagawa, T.L.D.R., Yanai, T., Sakai, H., 2013. The class a macrophage scavenger receptor CD204 is a useful immunohistochemical marker of canine histiocytic sarcoma. *J. Comp. Pathol.* 148, 188–196.

Liu, Y., Zhang, H.-P., Zhang, S.-F., Wang, J.-X., Zhou, H.-N., Zhang, F., Wang, Y.-M., Ma, L., Li, N., Hu, R.-L., 2016. Rabies outbreaks and vaccination in domestic camels and cattle in northwest China. *PLoS Negl. Trop. Dis.* 10, e0004890.

Pierezan, F., Mansell, J., Ambrus, A., Rodrigues Hoffmann, A., 2014. Immunohistochemical expression of ionized calcium binding adapter molecule 1 in cutaneous histiocytic proliferative, neoplastic and inflammatory disorders of dogs and cats. *J. Comp. Pathol.* 151, 347–351.

Poston, R.N., Hussain, I.F., 1993. The immunohistochemical heterogeneity of atheroma macrophages: comparison with lymphoid tissues suggests that recently blood-derived macrophages can be distinguished from longer-resident cells. *J. Histochem. Cytochem.* 41, 1503–1512.

Ramos-Vara, J.A., Miller, M.A., Valli, V.E., 2007. Immunohistochemical detection of multiple myeloma 1/interferon regulatory factor 4 (MUM1/IRF-4) in canine plasmacytoma: comparison with CD79a and CD20. *Vet. Pathol.* 44, 875–884.

Rasche, A., Saqib, M., Liljander, A.M., Bornstein, S., Zohaib, A., Renneker, S., Steinhagen, K., Wernery, R., Younan, M., Gluecks, I., Hilali, M., Musa, B.E., Jores, J., Wernery, U., Drexler, J.F., Drosten, C., Corman, V.M., 2016. Hepatitis e virus infection in dromedaries, north and east africa, United Arab Emirates, and Pakistan, 1983–2015. *Emerg. Infect. Dis.* 22, 1249–1252.

Raskin, R.E., 2016. Hemolymphatic system. In: Raskin, R.E., Meyer, D.J. (Eds.), *Canine and Feline Cytology*. W.B. Saunders, St. Louis, pp. 91–137.

Rehg, J.E., Bush, D., Ward, J.M., 2012. The utility of immunohistochemistry for the identification of hematopoietic and lymphoid cells in normal tissues and interpretation of proliferative and inflammatory lesions of mice and rats. *Toxicol. Pathol.* 40, 345–374.

Reusken, C.B.E.M., Haagmans, B.L., Müller, M.A., Gutierrez, C., Godeke, G.-J., Meyer, B., Muth, D., Raj, V.S., Vries, L.S.-D., Corman, V.M., Drexler, J.-F., Smits, S.L., El Tahir, Y.E., De Sousa, R., van Beek, J., Nowotny, N., van Maanen, K., Hidalgo-Hermoso, E., Bosch, B.-J., Rottier, P., Osterhaus, A., Gortázar-Schmidt, C., Drosten, C., Koopmans, M.P.G., 2013. Middle East respiratory syndrome coronavirus neutralising serum antibodies in dromedary camels: a comparative serological study. *Lancet Infect. Dis.* 13, 859–866.

Riek, A., Klinkert, A., Gerken, M., Hummel, J., Moors, E., Sudekum, K.H., 2013. Short communication: milk output in llamas (*Lama glama*) in relation to energy intake and water turnover measured by an isotope dilution technique. *J. Dairy Sci.* 96, 1815–1819.

Romero-Palomo, F., Rivalde, M.A., Molina, V., Sanchez-Cordon, P.J., Pedrera, M., Gomez-Villamandos, J.C., 2013. Immunohistochemical detection of dendritic cell markers in cattle. *Vet. Pathol.* 50, 1099–1108.

Rother, M.B., Schreurs, M.W., Kroek, R., Bartol, S.J., van Dongen, J.J., van Zelm, M.C., 2016. The human thymus is enriched for autoreactive B cells. *J. Immunol.* 197, 441–448.

Salvadori, C., Finlayson, J., Trogu, T., Formenti, N., Lanfranchi, P., Citterio, C., Palarea-Albaladejo, J., Poli, A., Chianini, F., 2016. Characterization of immune system cell subsets in fixed tissues from alpine chamois (*Rupicapra rupicapra*). *J. Comp. Pathol.* 155, 207–212.

Seibel, H., Stimmer, L., Siebert, U., Beineke, A., 2010. Immunohistochemical characterization of selected cell markers for the detection of hematopoietic cells in formalin-fixed, paraffin wax-embedded lymphoid tissues of harbor seals (*Phoca vitulina*) and walruses (*Odobenus rosmarus*). *Vet. Immunol. Immunopathol.* 137, 305–309.

Soulas, C., Conerly, C., Kim, W.-K., Burdo, T.H., Alvarez, X., Lackner, A.A., Williams, K.C., 2011. Recently infiltrating MAC387+ monocytes/macrophages: a third macrophage population involved in HIV and HIV encephalitic lesion formation. *Am. J. Pathol.* 178, 2121–2135.

Spencer, J., Choy, M., Hussell, T., Papadaki, L., Kington, J.P., Isaacson, P.G., 1992. Properties of human thymic B cells. *Immunology* 75, 596–600.

- Spitzbarth, I., Bock, P., Haist, V., Stein, V.M., Tipold, A., Wewetzer, K., Baumgärtner, W., Beineke, A., 2011. Prominent microglial activation in the early proinflammatory immune response in naturally occurring canine spinal cord injury. *J. Neuropathol. Exp. Neurol.* 70, 703–714.
- Steffen, D.J., Topliff, C.L., Schmitz, J.A., Kammerman, J.R., Henningson, J.N., Eskridge, K.M., Kelling, C.L., 2014. Distribution of lymphoid depletion and viral antigen in alpacas experimentally infected with Bovine viral diarrhoea virus 1. *J. Vet. Diagn. Investig.* 26, 35–41.
- Taylor, P.R., Martinez-Pomares, L., Stacey, M., Lin, H.H., Brown, G.D., Gordon, S., 2005. Macrophage receptors and immune recognition. *Annu. Rev. Immunol.* 23, 901–944.
- Theuß, T., Goerigk, D., Rasenberger, S., Starke, A., Schoon, H.A., 2014. Sektionsbefunde von Neuweltkameliden: Eine retrospektive Analyse des Sektionsgutes des Leipziger Instituts für Veterinär-Pathologie. *Tierarztl. Prax. Ausg. G Grosstiere Nutztiere* 42, 278–288.
- Tomokiyo, R.-I., Jinnouchi, K., Honda, M., Wada, Y., Hanada, N., Hiraoka, T., Suzuki, H., Kodama, T., Takahashi, K., Takeya, M., 2002. Production, characterization, and interspecies reactivities of monoclonal antibodies against human class A macrophage scavenger receptors. *Atherosclerosis* 161, 123–132.
- Vidana, B., Majo, N., Perez, M., Montoya, M., Martorell, J., Martinez, J., 2014. Immune system cells in healthy ferrets: an immunohistochemical study. *Vet. Pathol.* 51, 775–786.
- Vilafranca, M., Wohlsein, P., Trautwein, G., 1995. Expression of class II major histocompatibility complex molecules in renal tubular epithelial cells of canine kidneys affected with tubulointerstitial nephritis. *Res. Vet. Sci.* 59, 114–117.
- Wünschmann, A., Kremmer, E., Baumgärtner, W., 2000. Phenotypical characterization of T and B cell areas in lymphoid tissues of dogs with spontaneous distemper. *Vet. Immunol. Immunopathol.* 73, 83–98.
- Zaki, A.M., van Boheemen, S., Bestebroer, T.M., Osterhaus, A.D., Fouchier, R.A., 2012. Isolation of a novel coronavirus from a man with pneumonia in Saudi Arabia. *N. Engl. J. Med.* 367, 1814–1820.
- Zidan, M., Pabst, R., 2004. Histological, histochemical and immunohistochemical study of the haemal nodes of the dromedary camel. *Anat. Histol. Embryol.* 33, 284–289.
- Zidan, M., Pabst, R., 2012. Histological, histochemical and immunohistochemical study of the lymph nodes of the one humped camel (*Camelus dromedarius*). *Vet. Immunol. Immunopathol.* 145, 191–198.
- Zidan, M., Kassem, A., Dougbag, A., Ghazzawi, E.E., El Aziz, M.A., Pabst, R., 2000a. The spleen of the one humped camel (*Camelus dromedarius*) has a unique histological structure. *J. Anat.* 196, 425–432.
- Zidan, M., Schuberth, H.J., Pabst, R., 2000b. Immunohistology of the splenic compartments of the one humped camel (*Camelus dromedarius*). *Vet. Immunol. Immunopathol.* 74, 17–29.
- de Saint-Vis, B., Vincent, J., Vandenabeele, S., Vanbervliet, B., Pin, J.J., Ait-Yahia, S., Patel, S., Mattei, M.G., Banchereau, J., Zurawski, S., Davoust, J., Caux, C., Lebecque, S., 1998. A novel lysosome-associated membrane glycoprotein, DC-LAMP, induced upon DC maturation, is transiently expressed in MHC class II compartment. *Immunity* 9, 325–336.
- van Boheemen, S., de Graaf, M., Lauber, C., Bestebroer, T.M., Raj, V.S., Zaki, A.M., Osterhaus, A.D., Haagmans, B.L., Gorbalenya, A.E., Snijder, E.J., Fouchier, R.A., 2012. Genomic characterization of a newly discovered coronavirus associated with acute respiratory distress syndrome in humans. *MBio* 3, e00473–12.